

Kinetics of monolayer graphene growth by segregation on Pd(111)

H. S. Mok, A. Ebnonnasir, Y. Murata, S. Nie, K. F. McCarty, C. V. Ciobanu, and S. Kodambaka

Citation: *Applied Physics Letters* **104**, 101606 (2014); doi: 10.1063/1.4868386

View online: <http://dx.doi.org/10.1063/1.4868386>

View Table of Contents: <http://scitation.aip.org/content/aip/journal/apl/104/10?ver=pdfcov>

Published by the [AIP Publishing](#)

The advertisement features a dark blue background with a central image of the Model PS-100 probe station. On the left, the text 'NEW Model PS-100 Preconfigured Tabletop Probe Station' is written in white and orange. On the right, the Lake Shore CRYOTRONICS logo is shown, along with the tagline 'An affordable solution for a wide range of research' in a white, italicized font.

NEW
Model PS-100
Preconfigured Tabletop
Probe Station

 **Lake Shore**
CRYOTRONICS

*An affordable solution for
a wide range of research*



Kinetics of monolayer graphene growth by segregation on Pd(111)

H. S. Mok,¹ A. Ebnonnasir,² Y. Murata,¹ S. Nie,³ K. F. McCarty,³ C. V. Ciobanu,² and S. Kodambaka^{1,a)}

¹Department of Materials Science and Engineering, University of California Los Angeles, Los Angeles, California 90095, USA

²Department of Mechanical Engineering and Materials Science Program, Colorado School of Mines, Golden, Colorado 80401, USA

³Sandia National Laboratories, Livermore, California 94550, USA

(Received 26 January 2014; accepted 27 February 2014; published online 12 March 2014)

Using *in situ* low-energy electron microscopy and density functional theory calculations, we follow the growth of monolayer graphene on Pd(111) via surface segregation of bulk-dissolved carbon. Upon lowering the substrate temperature, nucleation of graphene begins on graphene-free Pd surface and continues to occur during graphene growth. Measurements of graphene growth rates and Pd surface work functions establish that this continued nucleation is due to increasing C adatom concentration on the Pd surface with time. We attribute this anomalous phenomenon to a large barrier for attachment of C adatoms to graphene coupled with a strong binding of the non-graphitic C to the Pd surface. © 2014 AIP Publishing LLC. [<http://dx.doi.org/10.1063/1.4868386>]

Among various methods of heteroepitaxial thin film growth, deposition from the bulk has attracted considerable attention in the recent years owing to interest in two-dimensional crystals such as graphene. In this approach, analogous to crystal growth from a liquid melt, material of interest diffuses out of the substrate upon cooling and forms a crystalline film on the substrate surface. For graphene-based devices, where graphene-metal contacts are necessary, dissolution of carbon into (and subsequent deposition from) the bulk of the metal can lead to undesirable layer thickness, quality (determined by the orientations and density of rotational domains), and hence electronic properties.¹⁻⁴ Therefore, a fundamental understanding of the mass transport mechanisms leading to the growth (and dissolution) of graphene via segregation from the bulk metal is essential for the development of large-scale graphene electronics. Here, we choose Pd, which has high solubility for carbon (~ 1.5 at. % at ~ 900 K)⁵ and is known to form the best electrical contact with graphene,⁶ and investigated the growth kinetics of graphene via segregation of C atoms from the bulk.

In the absence of an external carbon source, as in our experiments, the growth of graphene domains on the surface of a carbon containing Pd crystal involves two basic processes: (i) transport of C atoms from the bulk to the surface followed by and (ii) attachment of the C adatoms along the graphene domain edges. The nucleation density of graphene domains is controlled by the surface concentration C_{ad} of C adatoms, which depends on the rates of diffusion of C atoms to the surface and their incorporation into existing graphene domains. On Ru(0001), the rate-limiting step controlling graphene growth was found to be diffusion of C from the Ru crystal to its surface.⁷ As a consequence of slow diffusion, C_{ad} decreased after nucleation of graphene and resulted in low nucleation densities. Here, we find quite different behavior for the growth of graphene on Pd(111). Graphene

nucleation continues to occur until about one-half monolayer coverage. Individual graphene domains grow at a constant rate, indicating that their growth is controlled by the rate of C adatom attachment to the domain edges. Interestingly, the domains nucleating at later times are found to grow faster than those forming earlier, suggesting that C_{ad} increases with increasing time. We provide additional evidence in support of this unexpected increase in C_{ad} using electron reflectivity measurements and density functional theory (DFT) calculations of work functions $\Phi_{Pd}(t)$ of graphene-free Pd surfaces, which decrease by as much as 0.9 eV during graphene growth. Our results indicate that C adatoms are as stable as graphene on Pd(111) as a consequence of which extremely large concentrations of adatoms exist both during growth and dissolution of graphene. We attribute this phenomenon, previously not observed on other metals,^{8,9} to a combination of strong C-Pd binding energy and the presence of a barrier for attachment of C adatoms to graphene.

All the graphene growth experiments are carried out on a carbon-saturated Pd(111) single crystal in an ultra-high vacuum (UHV, base pressure $\sim 1 \times 10^{-10}$ Torr) LEEM system.¹⁰ Details of the sample preparation procedure are presented in Refs. 3 and 4. The substrate temperatures T are measured using a type-C thermocouple spot-welded to the sample. The sample is cooled from 960 °C to 880 °C at the rate of 1 K/s and held constant to facilitate the growth of monolayer graphene. Subsequent heating of the sample above the graphene growth temperature, for example, from 880 °C to 890 °C, leads to dissolution of the as-grown graphene layers. This approach enables multiple and reproducible growth experiments on the same sample and within the same regions of interest on the surface. Bright-field LEEM images are acquired at the rate of 2 frames/s while continuously varying the incident electron energy E between 0 and 6 eV in steps of 0.2 eV. Typical field of view is 20 μ m and pixel resolution in the images is 391 Å/pixel. Low-energy electron diffraction (LEED) patterns are obtained from the regions of interest and are used to identify the orientations of

^{a)}Author to whom correspondence should be addressed. Electronic mail: kodambaka@ucla.edu

graphene domains³ and the structure of non-graphitic carbon adsorbed on the surface.

LEEM image intensities $I(E,t)$ and the graphene domain sizes $R(t)$ are measured as a function of time t using ImageJ, an image processing software, as follows. At each E and t , $I(E,t)$ is determined as the spatial average of the intensities of all pixels within a given area. The $I(E,t)$ values are collected from three different regions and sizes ($195 \times 195 \text{ nm}^2$, $391 \times 391 \text{ nm}^2$, and $586 \times 586 \text{ nm}^2$) and checked for consistency. The sizes $R(t)$, defined as the square root of the sum total of all pixels within a graphene domain, are obtained from the images acquired at $E=6 \text{ eV}$, where graphene domains can be clearly distinguished from the bare Pd regions. The results presented here are representative of all of our measurements.

All of our DFT calculations are performed at the level of local-density approximation (LDA) using the double-zeta basis set and the Ceperley-Alder exchange correlation functional.¹¹ Both the atomic positions and the lattice vectors in the surface slabs are relaxed until residual forces fell below 0.04 eV/\AA , with an energy convergence tolerance of 10^{-5} eV for electronic structure calculations. The mesh cutoff is 250 Ry, the vacuum spacing is 15 \AA , and the Brillouin zone is sampled with $12 \times 12 \times 1$ grids during structural relaxations and with $30 \times 30 \times 1$ grids for single-point energy and Φ_{Pd} calculations. Given that Pd and C can form several carbides Pd_xC ,¹² and since random distributions of C adatoms either on Pd(111) or on Pd_xC phases with different surface orientations lead to a very large number of C/Pd structures, calculations for all the possible configurations at each concentration C_{ad} are computationally expensive and beyond the scope of the current report. Instead, we limit our DFT calculations to a smaller set of carbide-free Pd(111) surfaces, and the three relatively stable Pd_xC phases¹² with $x=1, 3$, and 6 , i.e., Pd_6C , Pd_3C , and rocksalt-structured PdC. The adsorption energy per C adatom, E_{ad} , is calculated as $E_{ad}(C_{ad}) = [N_{\text{Pd}}\mu_{\text{Pd}} + N_{\text{C}}\mu_{\text{C}} - E(C_{ad})]/N_{\text{C}}$, where N_i and μ_i (with $i = \text{Pd}$ or C) are the number and the chemical potential, respectively, of type i atoms, and $E(C_{ad})$ is the total energy of the relaxed structure at a given C_{ad} .

Figures 1(a)–1(d) are typical LEEM images acquired from a C-saturated Pd(111) sample during the growth of monolayer graphene at $T=895^\circ\text{C}$. Fig. 1(e) and the inset show time-dependent increases in the individual domain sizes $R(t)$ and the total areal coverage f_G of all the domains within the field of view, respectively. Within $t=50 \text{ s}$, graphene islands, the bright spots in Fig. 1(a), have nucleated; nucleation continues to occur until about one-half monolayer coverage of graphene. For example, the graphene domains 1, 2, and 3 highlighted by green, red, and blue circles nucleate $\sim 16 \text{ s}$, 50 s , and 91 s , respectively, after the initial nucleation. We find that the individual domains grow linearly with time, i.e., $R \propto t$. From the least-squares linear fits to the $R(t)$ data, we obtain the growth rates $dR/dt=0.01, 0.03$, and $0.06 \mu\text{m/s}$ for the domains 1, 2, and 3, respectively. That is, the domains nucleating at later times grow faster than their predecessors.

The constant growth rate dR/dt is consistent with attachment-limited kinetics,^{13,14} where areal growth rate dR^2/dt of the domain scales with its perimeter. (The underlying assumption is that the Gibbs-Thomson effect is negligible, which is valid for the large graphene domains observed in our experiments.) In comparison, for bulk diffusion limited growth of graphene, as observed on Ru(0001),⁸ R increases non-linearly with t as $R \propto t^{1/4}$. Attachment-limited growth kinetics are expected if (i) the bulk diffusivity of C atoms is sufficiently high and/or an ample supply of C atoms exists on or near the surface at all times, and (ii) there exists a barrier for the attachment of C atoms at the edges of graphene domains. The former criterion is likely satisfied, because we know from our previous experiments⁴ that multiple layers (>10) of graphene can be grown readily on our Pd(111) crystal by lowering the temperature. The latter condition is plausible as the growth of graphene on other metals required the attachment of C atom clusters rather than individual atoms.⁹ As noted earlier, the domain growth rate depends on its nucleation time. In order to explain this result, we propose that C_{ad} increases with t and justify our hypothesis below using electron reflectivity measurements and DFT calculations.

During graphene growth, we observed a drastic decrease in the image intensities $I(t)$ of graphene-free Pd regions. This

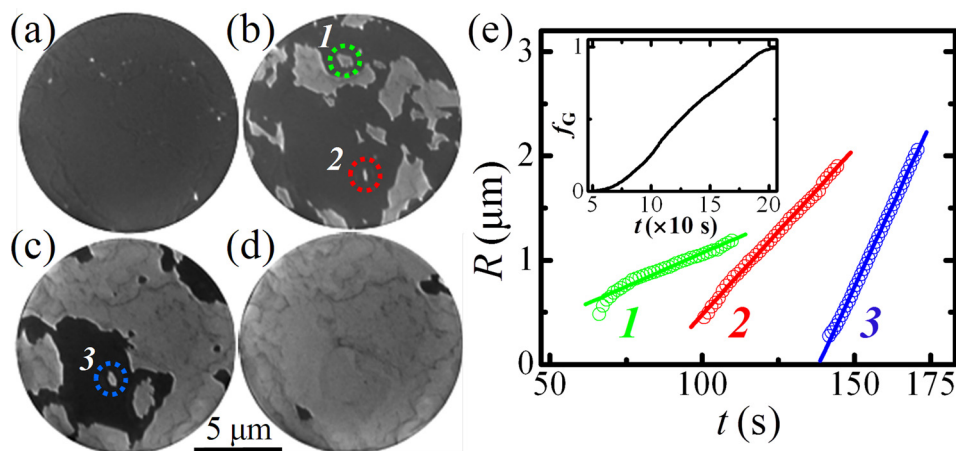


FIG. 1. Representative low-energy electron microscopy (LEEM) images acquired from a Pd(111) sample at times $t =$ (a) 50 s, (b) 100 s, (c) 150 s, and (d) 200 s during the growth of monolayer graphene (brighter grey contrast) at temperature $T=895^\circ\text{C}$ ($t \geq 50 \text{ s}$) upon cooling from $T=950^\circ\text{C}$ ($0 \leq t < 50 \text{ s}$). Field of view is $20 \mu\text{m}$ and incident electron energy $E=5 \text{ eV}$. The green, red, and blue circles highlight graphene domains 1, 2, and 3, respectively. Note the darkening of graphene-free Pd region contrast with time. (e) Plot of size R vs. t of the graphene domains 1, 2, and 3. Open symbols are measured data and solid lines are least-squares linear fits. Inset is a plot of the total areal coverage f_G vs. t of all the graphene domains in the field of view.

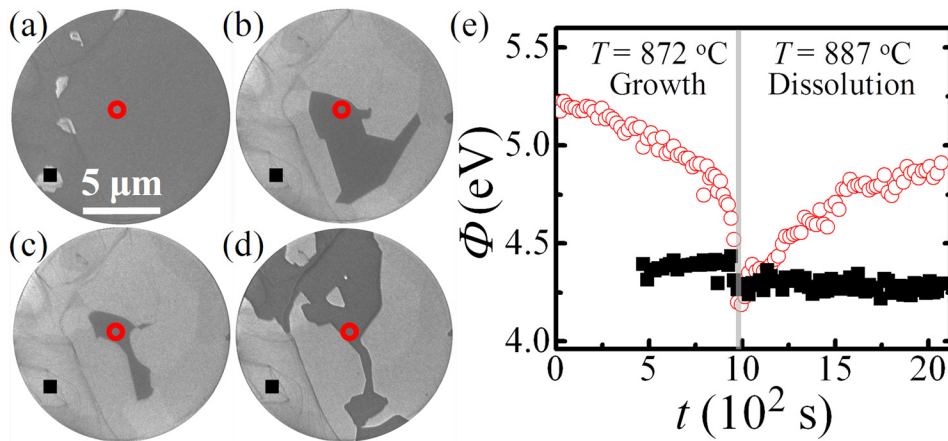


FIG. 2. (a)–(d) LEEM images (field of view = $20\ \mu\text{m}$ and $E = 6\text{ eV}$) obtained from the Pd(111) sample during growth at $T = 872^\circ\text{C}$ and $t =$ (a) 200 s and (b) 954 s, and dissolution at $T = 887^\circ\text{C}$ and $t =$ (c) 1100 s and (d) 2000 s of graphene domains (grey regions). In this experiment, $T = 887^\circ\text{C}$ at $t = 0$; 872°C at $100\text{ s} \leq t \leq 950\text{ s}$; and 887°C at $t \geq 970\text{ s}$. (e) Plots of work functions $\Phi_G(t)$ of graphene-covered (■) and $\Phi_{Pd}(t)$ of graphene-free (○) Pd(111) extracted from the solid black square and open red circle regions, respectively, highlighted in the LEEM images.

effect is readily seen in Fig. 1, in which the graphene-free Pd is light grey in (a), darker grey in (b), and almost black in (c). (For another example, see the LEEM images in Fig. S1 in supplementary material.¹⁵) From the measured $I(E, t)$ [see Fig. S2(a)], we extracted threshold energies needed to inject electrons into the surface^{3,4,16} and found that they decreased with increasing t during graphene growth at a constant T [see Fig. S2(b)]. In order to understand the origin of this phenomenon, we measured Φ_G of graphene-covered and Φ_{Pd} of graphene-free Pd regions from the LEEM images [see Figs. 2(a)–2(d)] acquired during growth and subsequent dissolution. Fig. 2(e) shows time-dependent variations in the Φ_G and Φ_{Pd} values measured from the same field of view. The data is collected following the procedure outlined in Refs. 3 and 4 and assuming that the work function of electron gun filament is 3.4 eV , which is accurate to within 0.3 eV . We find that Φ_G remains essentially constant at $\sim 4.3\text{ eV}$ at all times during graphene growth and dissolution processes. In contrast, Φ_{Pd} decreases from $\sim 5.3\text{ eV}$ to $\sim 4.5\text{ eV}$ with increasing time at the growth temperature; upon heating, as graphene begins to dissolve, Φ_{Pd} increases from $\sim 4.2\text{ eV}$ to $\sim 4.9\text{ eV}$. The difference in the final value (4.5 eV) measured at the growth temperature, and the initial value (4.2 eV) measured at the dissolution temperature is likely due to the time elapsed during the temperature change. In our experiments, the rate of change in Φ_{Pd} depends on both the substrate temperature and time. And the absolute values of Φ_{Pd} vary with the geometry of graphene domains and graphene-free regions in each experiment. The observed decrease (increase) in Φ_{Pd} with time during graphene growth (dissolution) at a given low (high) temperature is a direct indication that the surface or sub-surface composition of graphene-free regions is changing with time and that these changes can be reversed by increasing (decreasing) the temperature. In what follows, we provide evidence that this phenomenon can be explained by the accumulation of non-graphitic carbon, as C adatoms and possibly as carbidic phases (Pd_xC), in or under the Pd surface during graphene growth.

LEED data provide additional insight into the significant decrease in Φ_{Pd} during graphene growth. At the growth temperature, the LEED patterns of the graphene-free Pd contained only the same diffraction spots as clean Pd(111), as shown in Fig. S3(a). However, at lower temperature ($T = 37^\circ\text{C}$), we found additional spots corresponding to $(\sqrt{3} \times \sqrt{3})\text{ R}30^\circ$ structure [Fig. S3(b)]. This symmetry is commonly observed on close-packed metal surfaces covered by adsorbates with

repulsive interactions.¹⁷ We suggest that the observed surface structure is due to the presence of a high density of C adatoms on the Pd surface. The absence of additional LEED spots at the graphene growth temperature could result either from a lack of order or a lower density of C adatoms.

In order to understand the relationship between the measured Φ_{Pd} and the concentration C_{ad} of C adatoms in the vicinity of Pd(111), we turn to DFT. Fig. 3 shows the calculated Φ_{Pd} vs. C_{ad} for a few adatom configurations [e.g., Figs. S4(a)–S4(d)]. In these calculations, $C_{ad} = 100\%$ corresponds to one monolayer of graphene. For $C_{ad} \leq 40\%$, we obtain Φ_{Pd} values higher than that of pure Pd(111). However, at $C_{ad} \geq 50\%$, Φ_{Pd} is 0.5 to 0.9 eV below that of pure Pd(111) with the largest change (0.9 eV) observed for the adatom configuration with $C_{ad} = 50\%$ shown in Fig. S4(a). The presence of Pd_xC phases, with $x = 1, 3,$ and 6 , lowers the Φ_{Pd} a little ($\sim 0.05\text{ eV}$) with respect to that of the pure Pd(111). DFT calculations indicate that the rocksalt-structured PdC is unstable during surface slab relaxations; however, a single subsurface layer of C atoms in the rocksalt configuration is stable and reduces Φ_{Pd} by 0.15 eV . Clearly, surface carbides alone cannot account for the large ($\sim 0.9\text{ eV}$) decrease in Φ_{Pd} . Based upon our DFT calculations, we suggest that a large concentration of C adatoms, perhaps accompanied by surface carbides, can decrease Φ_{Pd} to the same extent as measured in our experiments.

Finally, we present a mechanism for the growth of graphene on Pd(111), schematically illustrated in Fig. 4. Since graphene layers grow upon cooling, at the growth temperature, C atoms will segregate to the surface and their surface

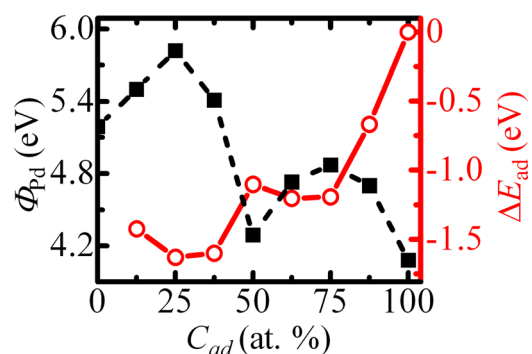


FIG. 3. Plots of calculated Φ_{Pd} (solid black squares) and C adatom adsorption energies ΔE_{ad} per C atom (open red circles) as a function of C adatom concentration C_{ad} . ΔE_{ad} is calculated with respect to the adsorption energy per C atom in graphene. The adatom configurations are shown in Fig. S4.

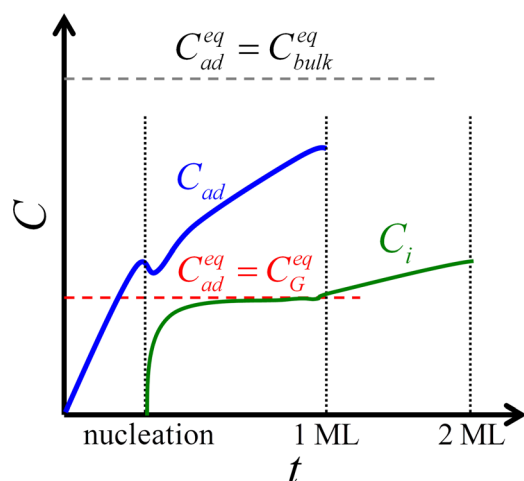


FIG. 4. Schematic of C concentrations during graphene growth on Pd via surface segregation of C atoms at a constant T . Even after the nucleation of graphene, C_{ad} (blue curve) continues to increase towards C_{ad}^{eq} , the value in equilibrium with the bulk carbon, C_{bulk}^{eq} (dashed grey line). Concentration C_i (green curve) of intercalated C begins to increase during monolayer growth, and when it sufficiently exceeds the value C_G^{eq} in equilibrium with graphene (the dashed red line), nucleation of the second graphene layer occurs.

concentration C_{ad} begins to increase with increasing time. At some critical C_{ad} , graphene domains nucleate and grow. If the rate of surface segregation of C atoms is higher than the rate of their incorporation into graphene, C_{ad} continues to increase as shown in Fig. 4 even after the initial nucleation. An additional factor that reduces the driving force to convert the adsorbed C into graphene and contributes to a high C_{ad} is the relatively small difference ΔE_{ad} between the adsorption energies per atom of non-graphitic C atoms on the surface and that of the C atoms in graphene [see the red curve in Fig. 3]. This process of increasing $C_{ad}(t)$ accounts for the higher growth rates for domains nucleating at later times and the decrease in Φ_{Pd} with time.

We now use Fig. 4 to describe multilayer graphene formation. As the monolayer graphene domains grow, C atoms begin to accumulate at the graphene/Pd interface. These intercalated C atoms are the primary source of multi-layer graphene growth.⁴ We expect that attachment of intercalated C atoms to the graphene edges is energetically more favorable than the attachment of C adatoms on the bare Pd and that the exchange of C between the bulk and the surface is fast. Under these conditions, the intercalated C atom concentration C_i quickly reaches the value in equilibrium with the graphene. Upon completion of the first monolayer growth, C_i begins to increase. (The absence of C_i signature in our electron reflectivity measurements of $\Phi_G(t)$ is consistent with this scenario.) At some critical concentration, the second layer of graphene nucleates and grows. As this process continues, multilayer graphene is obtained.

In summary, we investigated the kinetics of monolayer graphene growth via precipitation of carbon dissolved in a bulk Pd(111) crystal using a combination of *in situ* LEEM, electron reflectivity measurements, and DFT calculations. From the measurements of growth rates of individual graphene domains, we determined that there is a barrier for attaching C atoms to graphene and that the domains

nucleating later grow faster. And, work function of the graphene-free Pd decreases by up to 0.9 eV with increasing time. DFT calculations suggest that this work function change results from a high concentration of carbon adatoms, and possibly carbide phases, on the Pd surface. The ability of Pd(111) to accommodate a large concentration of non-graphitic C leads to an extended period of nucleation, while the presence of intercalated C atoms between graphene and Pd affects graphene-Pd coupling. The surface and intercalated C atom concentrations can vary with the annealing temperature as well as heating and cooling rates and can give rise to rotational domains. Since the domain density and orientations affect the strength of graphene-Pd interactions and hence the graphene-Pd contact characteristics, our studies provide insights into the role of thermal history on the performance of graphene-Pd contacts.

S.K. gratefully acknowledges the support from the Office of Naval Research (Dr. Chagaan Baatar) under Grant No. N00014-12-1-0518 and C.V.C. thanks the National Science Foundation for funding through Grant Nos. CMMI-0825592 and CMMI-0846858. Computational resources for this work were provided by the Golden Energy Computing Organization at Colorado School of Mines. Sandia work was supported by the Office of Basic Energy Sciences, Division of Materials Sciences and Engineering of the US DOE under Contract No. DE-AC04-94AL85000. We thank N. C. Bartelt for stimulating discussions and input, which helped formulate our ideas.

- ¹O. V. Yazyev and S. G. Louie, *Nature Mater.* **9**(10), 806–809 (2010).
- ²A. W. Tsen, L. Brown, M. P. Levendorf, F. Ghahari, P. Y. Huang, R. W. Havener, C. S. Ruiz-Vargas, D. A. Muller, P. Kim, and J. Park, *Science* **336**(6085), 1143–1146 (2012).
- ³Y. Murata, E. Starodub, B. B. Kappes, C. V. Ciobanu, N. C. Bartelt, K. F. McCarty, and S. Kodambaka, *Appl. Phys. Lett.* **97**(14), 143114 (2010).
- ⁴Y. Murata, S. Nie, A. Ebnonnasir, E. Starodub, B. B. Kappes, K. F. McCarty, C. V. Ciobanu, and S. Kodambaka, *Phys. Rev. B* **85**(20), 205443 (2012).
- ⁵T. B. Massalski, H. Okamoto, P. Subramanian, and L. Kacprzak, *Binary Alloy Phase Diagrams* (ASM international, 1990).
- ⁶F. Xia, V. Perebeinos, Y.-M. Lin, Y. Wu, and P. Avouris, *Nat. Nano* **6**(3), 179–184 (2011).
- ⁷K. F. McCarty, P. J. Feibelman, E. Loginova, and N. C. Bartelt, *Carbon* **47**(7), 1806–1813 (2009).
- ⁸E. Loginova, N. C. Bartelt, P. J. Feibelman, and K. F. McCarty, *New J. Phys.* **11**, 063046 (2009).
- ⁹E. Loginova, N. C. Bartelt, P. J. Feibelman, and K. F. McCarty, *New J. Phys.* **10**, 093026 (2008).
- ¹⁰K. F. McCarty, *Surf. Sci.* **474**(1), L165–L172 (2001).
- ¹¹J. M. Soler, E. Artacho, J. D. Gale, A. Garcia, J. Junquera, P. Ordejon, and D. Sanchez-Portal, *J. Phys.: Condens. Matter* **14**(11), 2745–2779 (2002).
- ¹²N. Seriani, F. Mittendorfer, and G. Kresse, *J. Chem. Phys.* **132**, 024711 (2010).
- ¹³J. G. McLean, B. Krishnamachari, D. Peale, E. Chason, J. P. Sethna, and B. Cooper, *Phys. Rev. B* **55**(3), 1811 (1997).
- ¹⁴S. Kodambaka, V. Petrova, S. V. Khare, D. Gall, A. Rockett, I. Petrov, and J. E. Greene, *Phys. Rev. Lett.* **89**(17), 176102 (2002).
- ¹⁵See supplementary material at <http://dx.doi.org/10.1063/1.4868386> for additional LEEM and LEED data.
- ¹⁶B. Unal, Y. Sato, K. F. McCarty, N. C. Bartelt, T. Duden, C. J. Jenks, A. K. Schmid, and P. A. Thiel, *J. Vac. Sci. Technol. A* **27**(5), 1249–1250 (2009).
- ¹⁷G. A. Somorjai, *Chemistry in Two Dimensions: Surfaces* (Cornell University Press, 1981).